Selective Targeting of the Retinal Pigment Epithelium in Rabbit Eyes with a Scanning Laser Beam

Carsten Framme,[1,2,3,4] *Clemens Alt,*[1,4,5] *Susanne Schnell,*[1,6] *Margaret Sherwood,*[1] *Ralf Brinkmann,*[2] *and Charles P. Lin*[1]

Purpose. Selective targeting of the retinal pigment epithelium (RPE) with repetitive laser pulses that minimize thermal damage to the adjacent photoreceptors is a promising new therapeutic modality for RPE-related retinal diseases. The selectivity of an alternative, more versatile scanning approach was examined in vivo by using a broad range of scanning parameters.

Methods. Acousto-optic deflectors repeatedly scanned the focus of a continuous wave (cw)-laser across the retina of Dutch belted rabbits, producing microsecond irradiation at each RPE cell. Two irradiation patterns forming separated lines (SEP) or interlaced lines (INT), different dwell times (2.5–75 μs), and repetition numbers (10 and 100 scans with 100-Hz repetition rate) were tested. Thresholds were evaluated by fundus imaging and angiography. Histology was performed for selected parameters.

Results. Selective RPE cell damage was obtained with moderate laser power. The angiographic threshold power decreased with pulse duration, number of exposures, and applying the INT pattern. Ophthalmoscopic thresholds, indicating onset of thermal coagulation, were higher than twice the angiographic threshold for most tested parameters. Histology confirmed selective RPE cell damage for SEP irradiation with 7.5 and 15 μs; slower scan speeds or closed lines caused photoreceptor damage.

Conclusions. A cw-laser scanner can be set up as a highly compact and versatile device. Selective RPE damage is feasible with dwell times up to 15 μs. Greatest selectivity is achieved with short exposure times and separated scan lines. Interlaced lines and long exposure times facilitate heat conduction into photoreceptors. A scanner is an attractive alternative for pulsed selective targeting, because both selective targeting and thermal photocoagulation can be realized. (*Invest Ophthalmol Vis Sci.* 2007;48:1782–1792) DOI:10.1167/iovs.06-0797

From the [1]Wellman Center for Photomedicine, Massachusetts General Hospital and Harvard Medical School, Boston, Massachusetts; the [2]Medical Laser Center Lübeck, Lübeck, Germany; the [3]University Eye Hospital Regensburg, Regensburg, Germany; the [5]Department of Biomedical Engineering, Tufts University, Medford, Massachusetts; and the [6]University of Applied Sciences Hamburg, Hamburg, Germany.

[4]Contributed equally to the work and therefore should be considered equivalent authors.

Supported by National Eye Institute EY12106 and by Lumenis, Inc.

Submitted for publication July 12, 2006; revised November 30, 2006; accepted January 19, 2007.

Disclosure: **C. Framme**, None; **C. Alt**, Lumenis (F); **S. Schnell**, None; **M. Sherwood**, None; **R. Brinkmann**, None; **C.P. Lin**, Lumenis (R)

The publication costs of this article were defrayed in part by page charge payment. This article must therefore be marked "*advertisement*" in accordance with 18 U.S.C. §1734 solely to indicate this fact.

Corresponding author: Charles P. Lin, Wellman Center for Photomedicine, Massachusetts General Hospital and Harvard Medical School, CPZN-8240, 185 Cambridge Street, Boston, MA, 02114; lin@helix.mgh.harvard.edu.

Retinal photocoagulation is one of the most well-established laser applications in medicine and is routinely performed in ophthalmic clinics worldwide. Conventional retinal laser photocoagulation is performed with a continuous wave (cw)–laser at 514 or 532 nm. The exposure times are typically 100 to 200 ms. An ophthalmoscopically visible grayish white lesion develops while the laser energy is applied to the retina, because of thermal denaturation and coagulation of the neurosensory retina. Histologically, destruction of the retinal pigment epithelium (RPE), the primary site of energy deposition, is accompanied by irreversible damage to the neuroretina's outer and inner segments caused by heat diffusion.[1–4]

Many retinal diseases, such as retinal detachment and diabetic retinopathy, are treated successfully by conventional laser irradiation. However, the benefit for the patient has to be considered carefully when macular irradiation is performed, because of the resultant laser scotoma that can lead to severe loss of visual acuity. Furthermore, the thermal destruction of photoreceptors does not contribute to the therapeutic effect in macular diseases that are caused by dysfunction of the RPE cells, such as drusen in early age-related macular degeneration (AMD), diabetic macular edema, and central serous retinopathy. Selectively destroying RPE cells while preserving the photoreceptors may be the appropriate treatment for these diseases.[5] The selective effect on RPE cells, that absorb approximately 50% of the incident green light,[6] due to their high melanosome content, was first demonstrated using 5-μs argon laser pulses at 514 nm, with a repetition rate of 500 Hz in experimental rabbit eyes.[5] Applying a train of brief, microsecond pulses that are on the order of the thermal relaxation time of the absorbing melanosomes (~1 μs) leads to high peak temperature or, depending on the exposure duration, to the formation of microbubbles[7–13] around the melanosomes. Subsequently, the RPE cells are destroyed, whereas the background temperature increase remains at sublethal levels.[14] Thus, collateral thermal damage is avoided, and photoreceptors remain intact as shown in various studies. Histology at different time points after irradiation demonstrated restoration of the blood–retinal barrier by proliferating and migrating RPE cells within 14 days after treatment.[5,14,15] Clinical trials in which an Nd:YLF laser system was used with a pulse duration of 1.7 μs (up to 100 pulses, 100 and 500 Hz) demonstrated the clinical potential of this technique, confirming by microperimetry that central vision is not adversely affected after selective targeting (Roider J et al. *IOVS* 1998;39:ARVO Abstract 104).[16]

With these promising initial results, it is imperative that a compact, reliable, clinically viable laser system be developed for selective RPE treatment so that the therapeutic benefits of this approach can be tested and established in a larger patient population. Unfortunately, such a laser system has not been available so far; the pulse laser system used by Roider et al. in the earlier studies are bulky, cumbersome benchtop devices.[15–17] Attempts to perform this treatment with a simple pulse diode laser source with 810 nm wavelength have been undertaken.[18–20] However, the attempts were unsuccessful in creating selective RPE lesions reproducibly, most likely because the wavelength and pulse duration of the diode laser were both

Investigative Ophthalmology & Visual Science, April 2007, Vol. 48, No. 4

suboptimal,[21] so that a temperature gradient between RPE and the adjacent tissue layers was not sufficiently established.[22]

We extensively tested the hypothesis that selective RPE damage can be created with a cw-laser in vivo, if the focused laser spot is rapidly scanned across the fundus so that each RPE cell just "sees" a microsecond pulse. A scanner, besides being a more compact alternative, has the ability to generate a variety of treatment parameters. By adjustment of scan speed (i.e., exposure time), repetition rate, and the shape of the scan pattern independently, treatment parameters can be optimized, and hypothetically the extent of selectivity can be controlled. The feasibility of scanning RPE cell targeting was demonstrated in preliminary ex vivo experiments employing a multimode-fiber–coupled Argon-ion laser scanner on sheets of porcine RPE.[23] The feasibility of scanning selective targeting was further demonstrated, using a Gaussian scanning beam, on sheets of bovine RPE and for selected scanning parameters in vivo.[24,25] In this study, we scrutinized the ability of a slit lamp–adapted laser scanner to create selective RPE lesions in the fundus of experimental rabbit eyes for a broad range of irradiation parameters. We evaluated the damage thresholds for various scan speeds, number of scans, and scan patterns by means of ophthalmoscopic and angiographic visibility. Furthermore considering the extent of selectivity by histologic examination, we identified several scanning parameters that are suitable for selective RPE targeting.

Material and Methods

Technical Design

We have developed a slit lamp–adapted laser scanner, as described in more detail elsewhere.[24] Briefly, the radiation of a frequency-doubled Nd:YVO_4 emitting at 532 nm (Verdi V-10; Coherent, Santa Clara, CA) was transmitted to the slit lamp adapted scanner via a polarization-maintaining (PM) single-mode fiber (Fibercore, Southampton, UK). Preserving single mode characteristics of the laser light was needed to achieve a small spot size in the eye. The scanner device was designed by using a two-dimensional acousto-optic deflector (2D-AOD; model AOD 2-DS; Brimrose, Baltimore, MD) that required linearly polarized light. To focus the scanning first-order beam through a contact lens into the eye, a single achromatic lens was placed in its focal distance from the spacing between the two crystals of the 2D-AOD, forming a nearly telecentric optic. The use of a PM fiber and losses due to diffraction efficiency of the 2D-AOD limited the available power at the cornea to a maximum of 180 to 185 mW.

The scanner device was mounted on top of an ophthalmic slit lamp (SL-130; Carl Zeiss Meditec GmbH, Oberkochen, Germany). The focal plane of the scanner was carefully adjusted to coincide with the object plane of the slit lamp. Thus, the slit lamp served as the targeting device for both aiming within the fundus and focusing the treatment beam.

Animals

In total, 20 Dutch belted rabbits were used for the experiments. Rabbits were chosen because the density and location of light-absorbing pigments in the fundus are rather uniform and similar to that of the human eye.[6] The rabbits were anesthetized with ketamine hydrochloride (35 mg/kg of body weight) and xylazine hydrochloride (5 mg/kg of body weight) and placed into a special holder system that allowed us to tilt and rotate the animal around its pupil in relation to the slit lamp. The experimental animals in this study were treated in compliance with the ARVO Statement for the Use of Animals in Ophthalmic and Vision Research.

Experimental Design

The laser beam (Gaussian profile) was focused through a Goldmann contact lens onto the central fundus' RPE in the rabbit eye by moving the retinal surface into the object plane of the slit lamp. The contact lens was locked to the animal holder to prevent unfavorable movements. The $1/e^2$-spot diameter in air was 27.5 μm. Calculations showed that the use of a planoconcave contact lens in cycloplegic emmetropic rabbit eyes leads to a magnification factor of 0.66.[26] Thus, the spot size in the retina was calculated to be 18.1 μm.

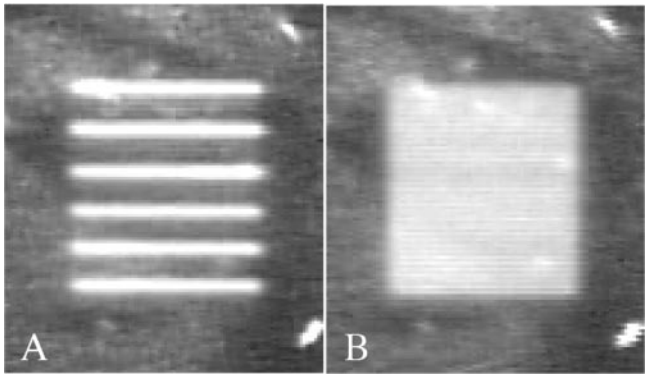

Figure 1. Irradiation pattern, generated by a single flying spot, with separated lines (termed SEP) (**A**) and with interlaced lines without spacing (termed INT) (**B**). Both patterns are 450 × 450 μm^2 in air in the rabbit retina. The spacing between line centers in the SEP pattern is 90 μm in air (60 μm in the rabbit retina). The INT pattern is composed of three interlaced SEP patterns that are displaced by one line. In this study, these patterns were applied repetitively 10 or 100 times at a rate of 100 Hz with various scan speeds.

In this study, irradiation was performed with two different scan patterns: The first scan pattern consisted of six separated lines (referred to as SEP) that were spaced approximately 60 μm apart (Fig. 1A). The second pattern consisted of 21 interlaced lines without spacing (referred to as INT; Fig. 1B). Both patterns illuminated a square field of approximately 300 μm length in the retina.

All experiments were conducted by applying one of these two scan patterns with identical, repetitive exposures at a rate of 100 Hz. The effect of exposure time on the threshold and the extent of selectivity was tested by 10 repetitive applications of the SEP pattern with 2.5-, 7.5-, 15-, 30-, 45-, and 75-μs dwell times (Table 1). Of these, 7.5 and 15 μs were also applied with 100 repetitive exposures, to observe the influence of increasing the number of repetitions (Table 2). To investigate the effects of the shape of the scan pattern, we applied the INT scan pattern with 10 repetitions of 7.5-μs and 100 repetitions of 15-μs dwell times as the presumably least and most invasive, potentially clinically useful parameters, respectively (Table 3).

All combinations of the parameters were tested in duplicates at various power levels, to determine the 50% effective dose (ED_{50})—that is, the light dose that would lead to RPE cell damage with 50% probability. Thus, the damage thresholds (ED_{50}) for each parameter were evaluated in two eyes of different animals. Corresponding radiant exposures in the center of the scan line were calculated based on the 18.1 μm spot size on the retina, and the scan speed as outlined by Brinkmann et al.[23] All tested parameters and their respective thresholds are summarized in Tables 1, 2, and 3.

ED_{50} Determination

Lesions were placed in the posterior retina by adjusting the slit lamp to allow the laser beam to enter the eye centrally. Visible suprathreshold marker lesions were used in all eyes to orient the particular nonvisible, selective laser scans. Marker lesions were placed by purposely causing coagulation of the neuroretina, using 100 scans at a 30-μs dwell time with 100-mW power. The test scans with various power levels were placed in the grid formed by these marker lesions. Approximately 30 test lesions were made in each eye (low 23, high 39), to determine the ED_{50}. Ophthalmoscopic visibility, manifested by the whitening of the retina, suggests thermal denaturation. It also marks the ophthalmo-

TABLE 1. Dependence of Angiographic Thresholds and Therapeutic Window on the Scan Speed for 10 Repetitive Exposures Using the SEP Pattern

	Angiographic Probability Analysis			Ophthalmoscopic Probability Analysis			
Exposure Time (μs)	ED_{50} Power (mW)	ED_{50} Fluence (mJ/cm^2)	Slope ED_{85}/ED_{50}	ED_{50} Power (mW)	ED_{50} Fluence (mJ/cm^2)	Slope ED_{85}/ED_{50}	TW
2.5	157	191	1.05	(>185)	−/−	−/−	−/−
7.5	87	318	1.11	(>180)	−/−	−/−	−/−
15	68	497	1.13	(>185)	−/−	−/−	−/−
30	40	585	1.01	140	2046	1.08	3.3
45	39	855	1.2	105	2302	1.07	2.2
75	35	1279	1.2	70	2557	1.01	1.6

Slope is that of the dose response curve for angiographic cell damage and ophthalmoscopically visible coagulation, respectively (ED_{85}/ED_{50}); TW, therapeutic window (ophthalmoscopic ED_{15}/angiographic ED_{85}).

scopic endpoint for this study. Ophthalmoscopic visibility was judged as positive or negative within moments after irradiation (Fig. 2B). Thirty minutes after treatment, fluorescein angiography with injection of 10% fluorescein sodium into the ear vein was performed with fundus camera (Carl Zeiss Meditec GmbH, Oberkochen, Germany). If the RPE is damaged, the distal blood–ocular barrier, formed by RPE and Bruch's membrane, will be compromised, and fluorescein can pool from the choriocapillaris into the subretinal space (Figs. 2A, 2C). Thus, fluorescein angiography was used to detect laser-mediated damage to the blood–ocular barrier, which defines the angiographic endpoint.

Experimental outcome was evaluated based on these two endpoints: The angiographic appearance of lesions suggested successful RPE cell damage (angiographic ED_{50}), whereas the ophthalmoscopic visibility of the lesion (ophthalmoscopic ED_{50}) suggested coagulation of the neural retina. The angiographic and ophthalmoscopic thresholds (ED_{50}) were calculated by using software for probit analysis (provided by Clarence P. Cain).[27] In probit analysis, the percentage of targets that respond to a given dose (in units of milliwatts or millijoules per square centimeter) is plotted against that dose by calculation of the lognormal fit through the quantal response data (dose–response curve; Fig. 3). For the computation, 1 was entered as soon as lesions became angiographically or ophthalmoscopically visible; 0 was entered when the respective endpoint was not reached. ED_{50} is that dose at which the dose–response curve crosses the 50% probability for the respective endpoint.

The therapeutic window (TW) is defined as the ratio of ophthalmoscopic ED_{15} over angiographic ED_{85}. It effectively constitutes a safety margin between a high probability of the desired effect (i.e., angiographically visible RPE damage) and a low probability of the unwanted side-effect (retinal thermal coagulation; ophthalmoscopically visible damage).

Histology

Selected parameters (10 and 100 repetitions of 7.5 and 15 μs SEP, 10 repetitions of 30 μs SEP, and 10 repetitions of 7.5 μs INT and 100 repetitions of 15 μs INT) were tested in two additional eyes after thresholds had been determined. Irradiation in each eye was systematically performed with four different doses based on previously measured angiographic thresholds (0.5× ED_{50}, 1× ED_{50}, 1.5× ED_{50}, and 2× ED_{50}). One parameter per eye was covered with 16 test scans (4 per dose), placed adjacent to the marker lesions. Resultant lesions were examined by slit lamp (ophthalmoscopic visibility), and fluorescein angiography (angiographic visibility). In addition, lesions were sectioned and the histology examined by light microscopy.

Eyes for histologic examination were enucleated in vivo in rabbits under deep anesthesia 1 hour after treatment. Immediately after enucleation, the globes were incised anterior to the equator and immersed in Karnovksy's solution. Twenty-four hours later, the posterior eyecup was cut from the anterior segment and the globe immersed in fresh fixative overnight. The areas of interest (marker lesions and lased lesions of the retina) were dissected and placed in fresh fixative for another 24 hours. The lesions were then postfixed in osmium tetroxide, dehydrated in a series of alcohols, and embedded in resin (Epon 812). Thick (1 μm) serial sections were cut through the lesion with a microtome (Ultracut E; Reichert, Vienna, Austria) and stained with methylene blue and toluidine blue.

RESULTS

Selective RPE damage was accomplished with a range of exposure parameters (see Tables 1, 2, and 3) involving a focused cw-laser beam that is rapidly scanned over the rabbit retina so that each RPE cell is irradiated with a microsecond exposure

TABLE 2. Dependence of Angiographic Thresholds and Therapeutic Window on the Number of Repetitions (All SEP)

	Angiographic Probability Analysis			Ophthalmoscopic Probability Analysis			
Parameter (Repetitions, Exposure Time)	ED_{50} Power (mW)	ED_{50} Fluence (mJ/cm^2)	Slope ED_{85}/ED_{50}	ED_{50} Power (mW)	ED_{50} Fluence (mJ/cm^2)	Slope ED_{85}/ED_{50}	TW
10× 7.5 μs	*87*	*318*	*1.11*	*(>185)*	−/−	−/−	
100× 7.5 μs	66	241	1.12	(>180)	−/−	−/−	
10× 15 μs	*68*	*497*	*1.13*	*(>185)*	−/−	−/−	
100× 15 μs	55	402	1.09	(>185)	−/−	−/−	(> 3.1)

Italic data are the same as from Table 1. No coagulation of photoreceptors was observed; consequently, a therapeutic window could not be determined. For the most invasive parameter, the therapeutic window is given as the minimum derived from the highest power tested versus the angiographic ED_{85}. Data are as described in Table 1.

TABLE 3. Dependence of Angiographic Threshold and Therapeutic Window on the Scan Pattern (SEP versus INT) for 10 Repetitions of 7.5-μs Exposure and 100 Repetitions of 15-μs Exposure

Parameter (Repetitions, Exposure Time, Pattern)	Angiographic Probability Analysis			Ophthalmoscopic Probability Analysis			
	ED_{50} Power (mW)	ED_{50} Fluence (mJ/cm^2)	Slope ED_{85}/ED_{50}	ED_{50} Power (mW)	ED_{50} Fluence (mJ/cm^2)	Slope ED_{85}/ED_{50}	TW
10× 7.5 μs SEP	*87*	*318*	*1.11*	*(>185)*	−/−	−/−	−/−
10× 7.5 μs INT	69	252	1.11	(>180)	−/−	−/−	−/−
100× 15 μs SEP	*55*	*402*	*1.09*	*(>185)*	−/−	−/−	−/− (>3.1)
100× 15 μs INT	45	325	1.11	70	511	1.01	1.5

Italic data and the remaining data description are the same as in Tables 1 and 2. Opthalmoscopically visible photocoagulation of photoreceptors was observed only with the most invasive parameter (100 repetitions of INT with 15-μs exposure time).

time. Visible marker (thermal) lesions were placed in the fundus, to document the treatment areas. Test lesions were placed between the marker lesions. Most of the treated areas were ophthalmoscopically invisible, indicating absence of thermal coagulation in the neurosensory retina. Damage to the RPE was visualized by fluorescein angiography (FLA) 30 minutes after the irradiation. At short exposure times (2.5 and 7.5 μs), none of the lesions was ophthalmoscopically visible, independent of the scan pattern and the number of repetitions, even when irradiated with the maximum available laser power of 185 mW entering the eye. With longer exposure times (15, 30, 45, and 75 μs), both selective lesions (i.e., visible only by fluorescein angiography) and nonselective lesions (visible by both fluorescein angiography and fundus ophthalmoscopy) were created (Fig. 2), depending on the laser power and scan pattern. Overall, successful RPE damage was routinely achieved in the posterior retina by adjusting the slit lamp so that the laser beam entered the eye centrally. In contrast, irradiation in the peripheral retina was not always successful, because of poor focusing. All results presented below are for central retina, as the current experiments were intended to test feasibility for treating macular disorders, such as diabetic macular edema, central serous retinopathy, and drusen macular degeneration with a scanning cw laser.

Threshold Determination

The thresholds for tested parameters were evaluated based on the angiographic and ophthalmoscopic visibility of the lesions as shown in Figure 2 (10 repetitions of 30 μs, SEP). Figure 2B shows the fundus as viewed through the slit lamp 2 hours after irradiation. Six prominent grayish white marker lesions (labeled M) formed a grid. Test lesions were placed in the area outlined by the markers, with laser power increasing from left to right. Lesions are not visible in the left half of Figure 2B (0 for ophthalmoscopic ED_{50} calculation), but become increasingly ophthalmoscopically visible with increasing laser power toward the far right (1 for ophthalmoscopic ED_{50} calculation). Fluorescein angiography (Figs. 2A, 2C) revealed where RPE cells were successfully damaged by the irradiation. Some lesions in the lower left of Figure 2A did not become visible (0 for angiographic ED_{50} calculation). In those, the applied dose was too low to cause any damage. In the same figure, other previously invisible test lesions appear (1 for angiographic ED_{50} calculation); those are selective lesions. In Figure 2C, lesions that were ophthalmoscopically visible in the slit lamp examination are also visible in fluorescein angiography. In the early phase of fluorescein angiography, lesions consistently appeared as separated hyperfluorescent lines that resembled the applied scan pattern. It is interesting to note that some lesions in Figure 2B —those lesions that are faintly visible between the reflections (r) and the top right marker—were not ophthalmoscopically visible immediately after irradiations. Those lesions were produced with a dose more than twice ED_{50} and began to appear only approximately 30 minutes after irradiation. The developing edema caused by irradiation leads to more significant visibility in this image (2 hours after irradiation).

Figure 3 shows the probability function for detecting positive lesions by fluorescein angiography and by ophthalmoscopy, using various scan speeds (indicated by the equivalent exposure time at the top of each panel), for 10 repetitions of the SEP scan pattern. For each exposure time, the damage probability is plotted as a function of increasing laser power. The top three panels (2.5-, 7.5-, and 15-μs exposure durations) show only the fluorescein angiographic results, because none of the lesions was ophthalmoscopically visible, even with maximum available laser power of 185 mW delivered to the eye. The bottom three panels (30, 45, and 75 μs) show both the

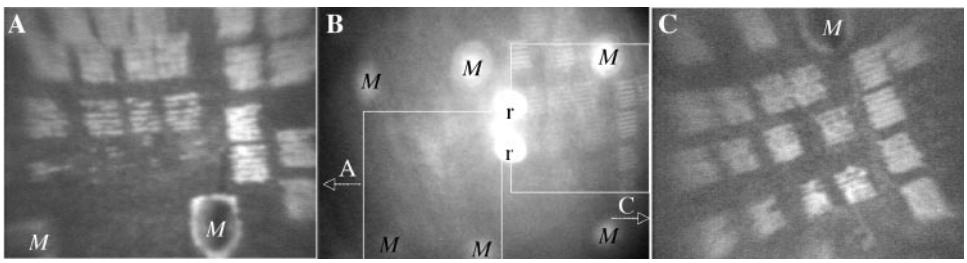

FIGURE 2. Determination of ED_{50} for 10 repetitive exposures of 30 μs with the SEP pattern. (**B**) Posterior fundus as seen through the slit lamp under white light illumination 2 hours after irradiation. Reflections from the contact lens (r) partially obstruct the view in the center of the image. Six ophthalmoscopically visible marker lesions (M) have been placed in a grid for orientation. Test lesions were applied between marker lesions with increasing power from *left* to *right*. The corresponding regions of the fluorescein angiography (FLA) (**A**, **C**) are outlined by *frames*. Lesions in the left half of the image (corresponding to **A**) were not ophthalmoscopically visible. Absence of visible coagulation suggests selectivity in those lesions. Some lesions toward the *right* of the image (corresponding to **C**) were ophthalmoscopically visible. This onset of coagulation that is visible in slit lamp examination immediately after irradiation serves as the endpoint to determine the ophthalmoscopic ED_{50}. Lesions become visible in fluorescein angiography (FLA) in those areas where RPE cells have been damaged due to irradiation. In the early phase of FLA separate individual hyperfluorescent lines can be distinguished (**A**, **C**). The onset of lesions that appear in FLA serves as the endpoint for determination of the angiographic ED_{50}.

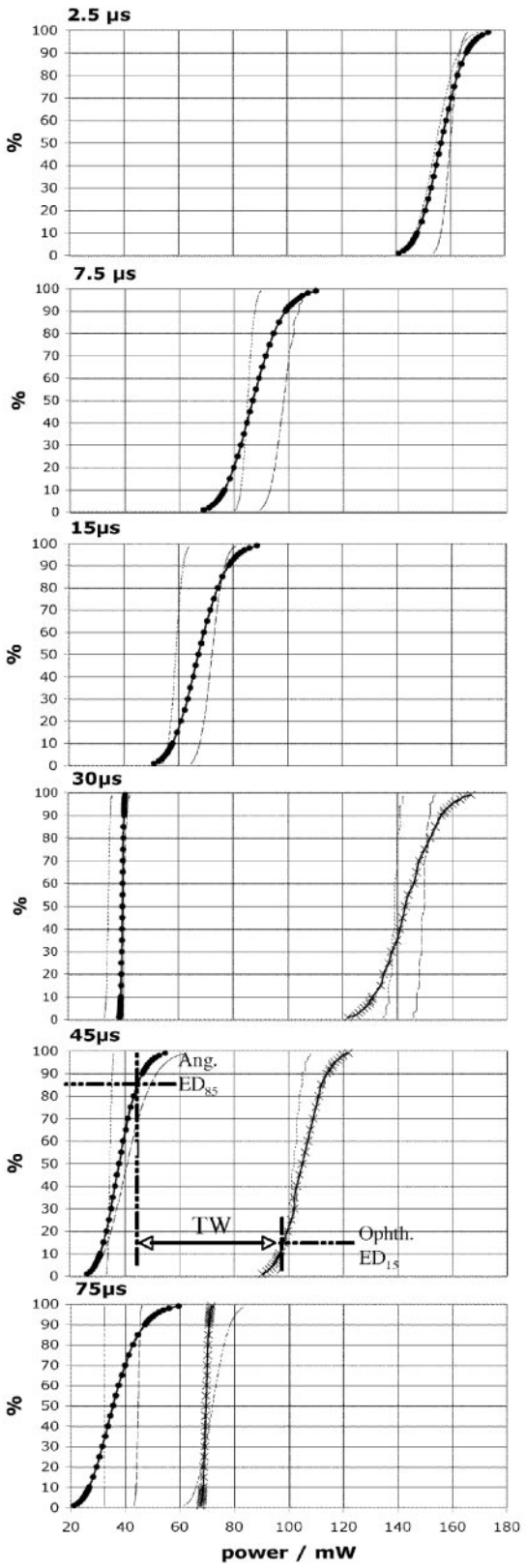

FIGURE 3. Angiographic (●) and ophthalmoscopic (X) damage probability as a function of power for 10 repetitions of the SEP scan pattern at various exposure times. Exposure time increases from *top* to *bottom*. All graphs are at the same scale, with the *right* end of the *x*-axis corresponding to the maximum available power on the cornea. *Heavy lines* with symbols: pooled dose responses from all lesions for each parameter; *dashed* and *dotted lines*: corresponding dose–response

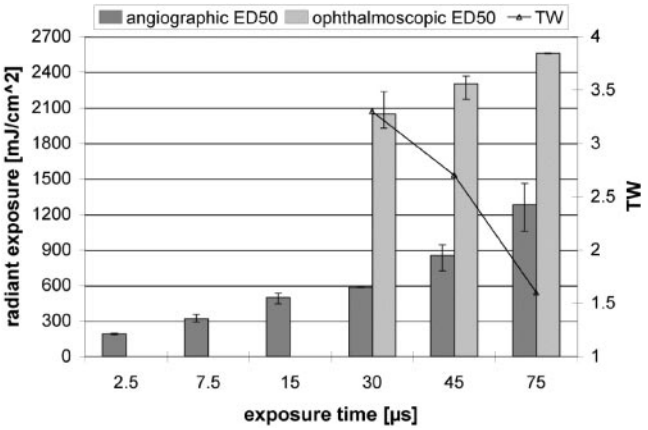

FIGURE 4. Dependence of angiographic and ophthalmoscopic ED_{50} radiant exposure on dwell time with 10 repetitions of the SEP pattern. Error bars represent the upper and lower limits of the 95% CI. Threshold radiant exposure increased with exposure duration for both angiographic and ophthalmoscopic damage, as heat diffusion becomes significant. Conversely, the therapeutic window increased as the exposure became shorter; although no ophthalmoscopically visible coagulation was observed for exposures shorter than 30 μs, the therapeutic window is expected to increase further as less energy was deposited into the tissue.

angiographic and ophthalmoscopic results. The gap between the 15% probability for ophthalmoscopically and 85% probability for angiographically visible damage is the therapeutic window. Its width decreases with increasing exposure time.

Dependence of RPE Damage Threshold on Irradiation Parameters

The probability curves of Figure 3 were calculated by the probit method. Thereby, the ED_{50} radiant exposures for angiographically and for ophthalmoscopically visible damage were determined. Figure 4 shows the ED_{50} radiant exposure plotted as a function of exposure time for 10 repetitive applications of the SEP pattern. With increasing dwell time (slower scan speed), the angiographic threshold power decreased while the threshold radiant exposure increased (Fig. 3, Table 1). The angiographic ED_{50} ranged from 191 mJ/cm^2 (157 mW) with 2.5 μs to 1279 mJ/cm^2 (35 mW) with 75-μs exposure durations. The ophthalmoscopic threshold was not reached for 2.5-, 7.5-, and 15-μs dwell times with the maximum available laser power of 185 mW. For 30-, 45- and 75-μs dwell times, the ophthalmoscopic thresholds were 2046, 2302, 2557 mJ/cm^2 (140, 105, and 70 mW), respectively. The ophthalmoscopic threshold was twice the angiographic threshold for 75-μs dwell time. This factor increased for shorter dwell times (up to 3.5- with 30-μs dwell time), indicating that for 10 scans of

from individual eyes. The power necessary to cause angiographic damage decreases with exposure time up to 30 μs. For exposure times longer than 30 μs, further decrease of threshold power becomes insignificant as heat diffusion increases. For up to 15-μs exposure time, visible coagulation of photoreceptors was not achieved. Ophthalmoscopic threshold was first reached using 30 μs. The width of the therapeutic window (TW; ophthalmoscopic ED_{15}/angiographic ED_{85}) decreases with exposure time from 3.3 with 30-μs exposures to 1.6 with 75-μs exposures. Slopes of probability functions from individual eyes, defined as ED_{85}/ED_{50} are, with one exception, always smaller than 1.1 for both angiographic and ophthalmoscopic dose responses, indicating a steep, step-like response. The slopes of pooled probability are consistently ~1.1, indicating little variation between the duplicate measurements.

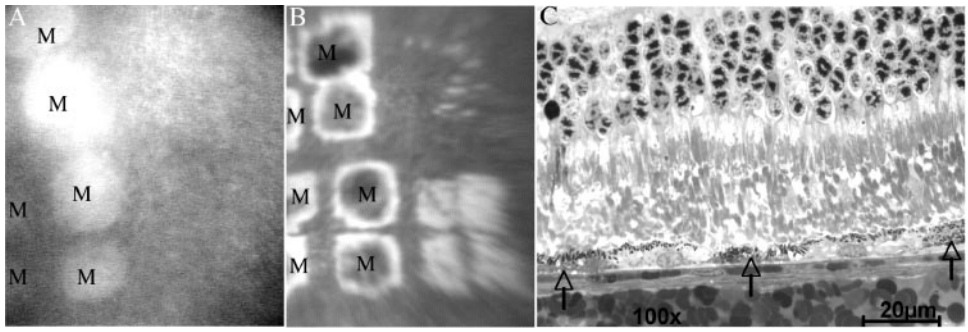

FIGURE 5. Fundus photograph (**A**), fluorescein angiography (**B**), and histologic section (**C**) of the same site in one eye after 100 repetitive 7.5-μs exposures employing the SEP pattern. (**A**) Posterior fundus as seen through the slit lamp under white light illumination immediately after irradiation. Test lesions were placed to the right of ophthalmoscopically visible marker lesions (M) with a dose corresponding to ED_{50} (top two markers) and with 2× ED_{50} next to the lower two markers. Absence of visible coagulation in slit lamp examination suggests selectivity of the test lesions. (**B**) Lesions became visible in fluorescein angiography. Lesions in the *top right* (1× ED_{50}) were partially visible. Lesions in the *bottom right* (2× ED_{50}) were fully visible; these lesions were sectioned perpendicularly to the scan lines for histologic examination. (**C**) Light microscopy of a histologic section of the 2× ED_{50} lesion. (**B**) *Arrows*: three dead RPE cells. The spacing between the damaged RPE cells corresponds to the distance between scan lines. RPE cells appear flat and condensed. Neighboring RPE cells and photoreceptors were not affected. With this exposure time, cell damage was confined to individual RPE cells in most of the cases and photoreceptors always appeared intact. M, thermal marker lesions.

separated scan lines, RPE cells can be safely targeted without visible neurosensory retina coagulation. The results for 10 repetitions of the SEP scan pattern are summarized in Table 1.

Table 2 shows that there is a small reduction in thresholds when the number of repetitive scans of the SEP pattern was increased from 10 to 100 (24% and 20% reduction for 7.5- and 15-μs dwell times, respectively). Despite a 10-fold increase in repetitive exposures, no lesions were ophthalmoscopically visible; the therapeutic window is at least 3.1 and 2.5 for 100 repetitions of 15- and 7.5-μs exposures (SEP).

Changing the scan pattern from separated to interlaced lines also caused a slight decrease in threshold, as shown in Table 3. No ophthalmoscopically visible damage was observed with 10 repetitive applications of the INT scan pattern for 7.5-μs dwell time. With 100 repetitions of the INT pattern with 15-μs exposures, however, ophthalmoscopically visible lesions were observed at a factor of 1.5 above angiographic ED_{50}. As described earlier, the same number of repetitions using the SEP pattern with 15-μs dwell time did not result in visible coagulation for radiant exposure of up to 3.1 times the angiographic ED_{50}.

Probit analysis further yields the slope of the dose–response curve, defined as ED_{85}/ED_{50} (Tables 1 2, and 3). The slopes of individual probability functions were, with one exception, always smaller than 1.1 for both angiographically and ophthalmoscopically visible damage, indicating a steep, step-like response (see also Fig. 3). The steep slope of individual dose–response curves suggests stable experimental conditions (e.g., focusing) for all test lesions in the same eye. The slope of pooled probability curves, considering all lesions of the same parameter, was approximately 1.1, indicating little variation between the duplicate measurements.[28]

Assessment of Cell Damage

Besides the evaluation of the outcome of irradiation by slit lamp examination and fluorescein angiography, the extent of selectivity of selected parameters was also assessed by histology. Results for 7.5- and 15-μs exposures confirmed that RPE cells were selectively damaged when these parameters were used (Figs. 5 and 6), consistent with the absence of visible coagulation for 10 and 100 repetitive applications of the SEP pattern. The damaged RPE cells were flat, with some of the debris lying on Bruch's membrane, and the melanin granules lost their apical orientation. There was no observable difference in the damage from irradiation with 10 or 100 repetitions at radiant exposure of one or two times angiographic threshold. Likewise, no damage was observed throughout the neural retina. The outer segments of the photoreceptors that are in contact with the RPE remained unaffected, showing preserved photoreceptor structure and orientation. In all sections, Bruch's membrane and choriocapillaris appeared intact.

In addition, histology of 7.5-μs dwell time with 100 repetitions of the SEP pattern frequently showed individually damaged RPE cells, even for the highest tested fluence of twice the ED_{50} (Fig. 5C). Damage was confined to the RPE cells; photoreceptors appeared normal. Individually damaged RPE cells were separated by the distance between the lines of the applied pattern. They were sharply demarcated from neighboring

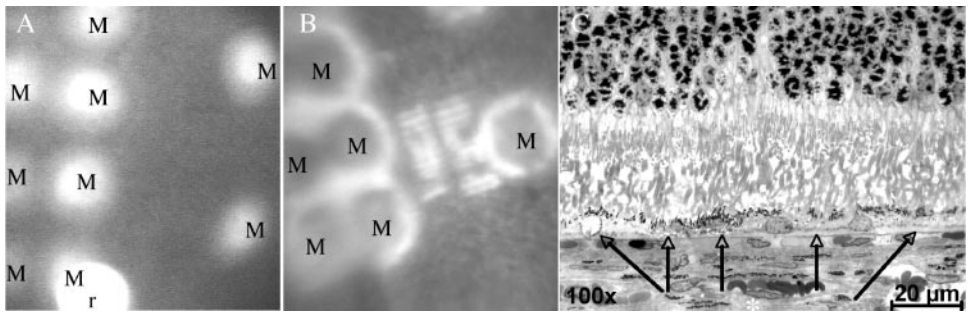

FIGURE 6. Fundus photograph (**A**), fluorescein angiography (**B**), and histologic section (**C**) of the same site in one eye after 100 repetitive 15-μs exposures employing the SEP pattern. (**A**) Posterior fundus as seen through the slit lamp under white light illumination immediately after irradiation. Test lesions were placed between *triangles* formed by markers (M). Test lesions with a dose of 2× ED_{50} were placed in the *bottom triangle*. Absence of visible coagulation suggests selectivity of the test lesions. (**B**) Previously invisible selective lesions of the 2× ED_{50} irradiation became visible in fluorescein angiography. Individual fluorescent lines can be distinguished. These lesions were sectioned perpendicular to the scan lines for histologic examination. (**C**) Image of the 2× ED_{50} lesion of (**B**). *Arrows:* several affected cells. RPE cell damage was confined to the RPE layer; the photoreceptors appeared unaltered. However, different from the 7.5-μs histology, damage was not necessarily confined to individual RPE cells; with this exposure time, neighboring RPE cells were more frequently affected. Furthermore, some coagulated red blood cells were found in the choriocapillaris adjacent to the RPE. M, thermal marker lesions; r, reflections from contact lens.

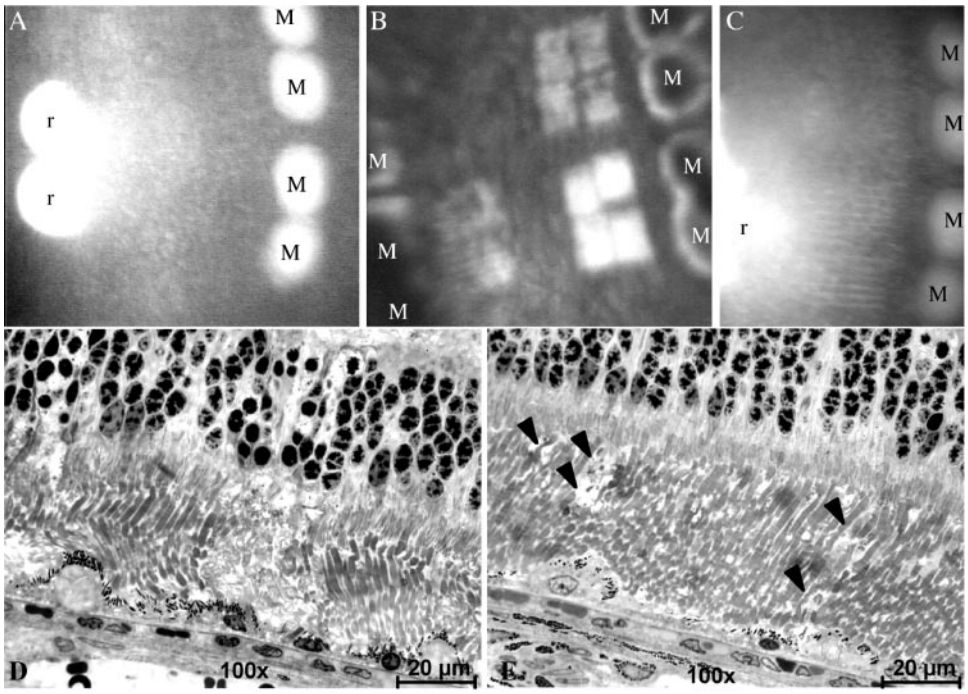

FIGURE 7. Fundus photograph 1 minute (**A**) and 30 minutes after irradiation (**C**), fluorescein angiography (**B**), and histologic sections (**D**, **E**) of the same site in one eye after 30-μs exposure with 10 repetitions employing the SEP pattern. None of the test lesions (2× ED_{50} *left* of *top* markers; 3× ED_{50} *left* of *bottom* markers) was ophthalmoscopically visible through slit lamp examination immediately after exposure (**A**) but were detected by fluorescein angiography (**B**). Also visible in (**B**) is the dose corresponding to ED_{50}. After 30 minutes, the edema developed in the 3× ED_{50} lesions, leading to faint visibility through the slit lamp (**C**). In histologic examination, photoreceptors appeared altered after irradiation with 3× ED_{50} (**D**). Separated damage in the photoreceptors is spaced corresponding to the distance between scan lines. The coagulation extends through the outer segments into the nuclear layer of the photoreceptors. Blood vessels of the choroid seem to be intact, but red blood cells are denatured. Reduction of the irradiation to 2× ED_{50} reduces the significance of photoreceptor damage (**E**). RPE cells that appear normal are rarely found, and occasional damage to photoreceptors remains (*arrows*). Note that virtually all red blood cells in (**D**) and (**E**) have been coagulated. M, thermal marker lesions; r, reflections from contact lens.

RPE cells that appeared intact. In those surviving RPE cells, the nuclei were clearly visible and the melanosomes were still arranged as a shield apical to the nucleus.

Similar results were obtained in histology after irradiation with 100 repetitions of the SEP pattern with 15-μs dwell times (Fig. 6C). The cell damage was confined to the RPE cell layer and photoreceptors were preserved, even after irradiation with radiant exposure twice the ED_{50}. However, damage to individual RPE cells was rarely found. Neighboring RPE cells were more frequently affected so that the origin of the initial laser impact often could not be determined.

Histology of irradiation at radiant exposure three times angiographic ED_{50} of 30-μs dwell time (10 repetitions, SEP) showed photoreceptors that appeared significantly altered in the area of laser impact (Fig. 7D), although the therapeutic window was measured to be 3.3 at this laser setting. The damage extended through the outer segments of the photoreceptors into the nuclear layer of the photoreceptors but was not visible in slit lamp examination (Fig. 7A); however, edema was observed in these lesions after 30 minutes (Fig. 7C). Reducing the radiant exposure to twice the ED_{50} reduced the extent of the photoreceptor disturbance. Here, damage was mostly confined to the RPE cell layer. However, surviving RPE cells became rare, and isolated pockets of photoreceptor damage were still found (Fig. 7E). Many coagulated red blood cells were found in the choroid; however, bleeding through Bruch's membrane was not observed.

Irradiation with 100 repetitions of the INT pattern with 15-μs scan speed at a radiant exposure of twice angiographic ED_{50} led to photoreceptor coagulation that was visible in the slit lamp examination immediately after irradiation (Fig. 8A). Both 2×-ED_{50} and 1.5×-ED_{50} lesions developed edema within 30 minutes after irradiation (Fig. 8C). Histology of the 1.5× ED_{50} lesion confirmed continuous RPE cell damage adjacent to a bridge of surviving cells between the two lesions. Although the photoreceptors appear morphologically normal, they are actually "distorted," due to the edema. Within the lesion, the RPE was flat and condensed and photoreceptors appeared to be intact throughout the lesions (Fig. 8D).

DISCUSSION

Currently, age-related macular degeneration and diabetic retinopathy are the leading causes of blindness in the developed world. Laser photocoagulation is performed routinely to alleviate signs and symptoms of retinal diseases and to prevent sight-threatening complications. However, the bystander damage to the photoreceptors by conventional laser photocoagulation is extensive and visually detrimental. To achieve therapeutic retinal targeting and minimize bystander damage, Birngruber and Roider pioneered selective targeting of the RPE by using brief, microsecond pulses.[5,14] The therapeutic effect of selective laser treatment in several macular diseases is attributed to the migration and proliferation of surviving RPE cells adjacent to the lesion, leading to a restored blood–retinal barrier and an enhanced pump function of the RPE layer[5,14,29,30] that may be able to remove existing edema or drusen. Targeting the RPE cells with repetitive microsecond pulses has been shown, both in preclinical and clinical pilot studies, to produce the desired RPE damage while avoiding laser scotoma (Roider J et al. *IOVS* 1998;39:ARVO Abstract 104).[5,14–16] However, the lasers creating the required pulse structure are large, maintenance-intensive benchtop devices that may not be practical in routine clinical operations.

We are currently developing a new technique for selectively targeting the RPE by scanning a focused cw-laser beam[24] rapidly across the retina. The scanning paradigm creates short exposure durations without the need for a complex pulse laser source. By applying separated (SEP) scan lines on ex vivo bovine RPE flatmounts in a prior study, we obtained alternating lines of damaged and intact RPE cells that replicate the applied scan pattern, indicating damage confinement to the irradiated cells.[24] We also showed, by means of fundus photography and fluorescein angiography in rabbits, that selective targeting is

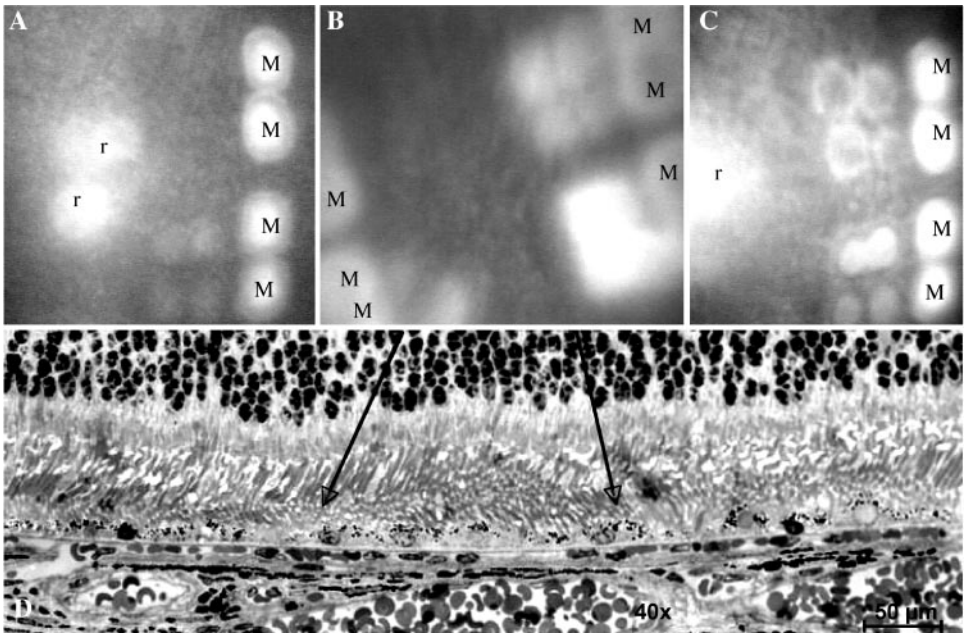

FIGURE 8. Fundus photograph 1 minute (**A**) and 30 minutes after irradiation (**C**), fluorescein angiography (**B**), and histology (**D**) of the same site in one eye after 100 repetitive applications of the INT pattern with 15-μs dwell time. Test lesions with 1.5× ED_{50} (*left* of *top* markers in **A**) are not ophthalmoscopically visible; 2× times ED_{50} led to coagulation immediately after treatment (*left* of *bottom* markers in **A**). Both parameters became visible in FLA (**B**). Also, the dose corresponding to ED_{50} is partially visible in the lower left of (**B**). Edema developed in lesions produced with 1.5× and 2× ED_{50}, yielding enhanced visibility in slit lamp examination 30 minutes after treatment (**C**). Histology of the 1.5× ED_{50} lesion confirmed damage to RPE cells (**D**). Signs of coagulation of photoreceptors were not found. Their size and shape seemed to be intact; however, the photoreceptor layer appeared "distorted" by the edema. The two lesions were separated by a bridge of surviving cells (*arrows*). M, thermal marker lesions; r, reflections from contact lens.

feasible in vivo using 7.5- and 15-μs exposure durations. However, fundus photography and fluorescein angiography alone were not sufficient to assess whether damage was strictly confined to the RPE layer. Recently, we presented preliminary histologic finding of selective RPE damage in vivo after exposure to a single scanning parameter (5 μs, SEP scan pattern). Selectively damaged RPE cells were seen next to intact photoreceptors for this treatment parameter.[25]

We have extended these studies to cover a much broader range of exposure parameters, extending from exposure times on the order of the thermal relaxation time of the absorbing structures (2.5 μs) to well beyond that regimen (up to 75 μs). These studies are important because in designing a scanning system for clinical applications, one has to take into account not only the requirement to achieve selectivity with a sufficiently large safety margin (i.e., therapeutic window), but also the need to have a reasonably compact and inexpensive instrument. As shown in Figure 3, the therapeutic window clearly increases with decreasing exposure duration. However, the increase in therapeutic window comes at the expense of increasing laser power, with accompanying increase in system cost and bulkiness. As the advances in laser technology will inevitably drive down both size and cost, the comprehensive results presented herein will provide useful guidelines for future system design considerations with regard to available laser source and the achievable selectivity. Moreover, from a clinical perspective, it may be beneficial to have the ability to control the degree of selectivity during treatment with a single instrument. By adjusting the scan speed and/or scan pattern, it is possible to produce either selective RPE damage (Figs. 5C, 6C) or nonselective (thermal) lesions that extend to the photoreceptors (Figs. 7D, 8A). This flexibility is a key feature of the scanning approach. For the highest degree of selectivity, damage to individual RPE cells can be achieved. Given this microscopic precision of the scanner, future laser treatment of central retinal diseases may be possible even in the fovea if a suitable feedback mechanism, such as the detection of microscopic intracellular bubbles, is used. In contrast, thermal coagulation can be realized with the same device by adjusting scanning parameters to facilitate heat diffusion into the neural retinal layers, for instance by slowing down the scan speed or by scanning without spacing between adjacent scan lines (the INT scan pattern). Thus, a laser scanner is a compact and reliable device for RPE targeting that can allow the laser treatment to be tailored to individual patients' retinal disease.

In our scanning device, the radiation of the cw-laser is delivered to a slit lamp mounted scanning unit with an optical fiber. We scan a laser spot about the size of one RPE cell across the retinal surface with a speed such that every targeted cell will be irradiated with microsecond exposure. Selective cell damage was demonstrated with moderate laser power (on the order of 100 mW) by the appearance of lesions in fluorescein angiography with concurrent absence of ophthalmoscopically visible coagulation. For most of the parameters tested, photoreceptor coagulation was not achieved even with irradiation far above angiographic threshold. Histology of 7.5- to 15-μs exposure times with the SEP pattern confirmed microscopically the absence of damage to the photoreceptor layer; thus, selectivity was substantiated for these laser settings. Histology for 2.5-μs exposure was not performed; however, it is reasonable to expect the photoreceptors to be preserved by using a shorter exposure time (i.e., better thermal confinement to the RPE) with lower radiant exposure (Table 1). Subtle damage to the photoreceptors may not be visible in light microscopy (Fig.

7). However, it is known that restoration of the photoreceptor outer segments is possible as long as the cell nuclei remain intact. Roider et al.[18] (Roider J et al. *IOVS* 1998;39:ARVO Abstract 104) have shown in trials in which microperimetry was used in patients that the full field of view recovered within 1 week to 3 months after initial detection of a small number of blind spots after selective RPE treatment.

Dependence of Cell Damage Thresholds on Irradiation Parameters

We observed in our experiments using 10 repetitive exposures with the SEP pattern that the angiographic ED_{50} radiant exposure increased with exposure time, whereas the angiographic ED_{50} power decreased (Table 1). If laser energy is applied within the thermal relaxation time of the melanosomes (~1 μs), heat diffusion is minimized, and the temperature is confined to the absorber. With increasing exposure times, heat diffusion becomes significant, and, thus, higher radiant exposure was necessary to replace the amount of heat energy that dissipated during the exposure.

The slight reduction of the RPE damage thresholds due to application of 100 repetitions of the SEP pattern (Table 2) can be explained by the fact that the 100-Hz repetition frequency may be too high to allow the tissue in the irradiated area to cool completely to body temperature. Thus, heat gradually accumulates over a large number of repetitions, leading to a lower measured damage threshold.

Irradiation with the INT pattern was markedly different from that with the SEP pattern. Lower angiographic thresholds were measured for both 7.5-μs (10 repetitions) and 15-μs exposures (100 repetitions; Table 3). At the 15-μs dwell time ophthalmoscopically visible coagulation of the neural retina was also observed. Applying the INT pattern (21 lines without spacing) versus the SEP pattern (six spaced lines) introduces two effects. First, the total energy applied to the tissue is higher as the duty cycle increases (for 15-μs dwell time, the duty cycle approached 55% in INT versus 15% in 15-μs SEP). Second, because adjacent lines in the INT pattern were produced with a time delay of approximately 3 ms, thermal energy that diffused away from the flying spot while the scan was in progress heated up adjacent target areas, yielding a lower threshold.

Dependence of Therapeutic Window on Irradiation Parameters

For selective laser treatment, a safety margin between the angiographic and the ophthalmoscopic threshold is crucial to the prevention of unintentional photoreceptor cell damage. To ensure that most targeted RPE cells are damaged, irradiation above angiographic ED_{50} is desirable, yet damage to photoreceptors is to be avoided. For this purpose, we define the safety margin as the ratio of ophthalmoscopic ED_{15} over angiographic ED_{85}. This safety margin is commonly referred to as the therapeutic window (TW). Because of the intra- and interindividual variation in pigmentation, which can differ by a factor of two in humans,[6] a therapeutic window as large as possible is desired in a clinical setting.

Varying only the scan speed while keeping other parameters constant, we were able to show that the therapeutic window increases for irradiation with decreasing exposure time for the SEP pattern from a factor of 1.6 (75-μs dwell time) to 3.3 (30-μs dwell time) (Figs. 3, 4; Table 1). We expect the therapeutic window to be even wider at shorter dwell times because less energy is applied to the retina and there is less heat diffusion away from the RPE. The therapeutic window was not determined for scan speeds between 2.5 and 15 μs because the available laser power was not sufficient to create ophthalmoscopically visible lesions. According to Figure 3, none of the angiographic 85% probability points overlapped with the ophthalmoscopic 15% points, even at exposure times that were significantly longer than the RPE thermal relaxation time. Angiographic ED_{100} was reached at approximately 30% above ED_{50} (Fig. 3). As confirmed by histology, there was no damage to photoreceptors observed with 10 and 100 repetitions of the SEP pattern, with 7.5-μs exposures (on the order of the thermal relaxation time), or even with a 15-μs dwell time (longer than the thermal relaxation time) at doses of up to twice ED_{50} (Figs. 5, 6).

It is interesting to note that 15-μs INT exposures had a much narrower therapeutic window (1.5) than did SEP exposures (Table 3). Heat diffusion geometry introduced by irradiation with separated scan lines can be modeled as separated cylinders, whereas heat distribution with INT exposure approximates a disc. The latter has greater heat conduction into the photoreceptors.

As expected, thermal coagulation that is seen by histology to be confined to the photoreceptors (i.e., not extending through the entire thickness of the retina) may not be visible in slit lamp examination (Fig. 7, 30-μs SEP). Therefore, the therapeutic window for 30-μs SEP exposure should be smaller than 3.3 indicated by the ophthalmoscopic and angiographic measurements. Furthermore, ophthalmoscopic lesions that are initially invisible can appear with time after irradiation, as has already been observed in the pulsed laser approach.[17] This was more likely when energies higher than angiographic threshold were applied (Figs. 2, 7, 8). Those lesions were not visible during the first 10 minutes after irradiation but became visible after 30 minutes. This late-onset visibility is attributed to damaged RPE that weakens the blood–retina barrier and leads to extracellular fluid leaking in those particular areas (i.e., edema). The change of the scattering properties of the neurosensory retina, due to the edema in the subretinal space, eventually leads to ophthalmoscopic visibility. In fact, leakage though the compromised blood–ocular barrier is the basis for fluorescein angiography, currently the standard method of detecting laser-mediated RPE cell damage. Just as lesions created with the INT pattern appear brighter in fluorescein angiography than those created with the SEP pattern, we observed the most significant edema in lesions that were created with the INT pattern above ED_{50} (Fig. 8). The total area of compromised barrier was larger in INT than in SEP, yielding a higher fluid diffusion rate into the subretinal space. Consequently, edema developed more quickly in INT than in SEP lesions. It is therefore imperative to judge ophthalmoscopic visibility within moments after irradiation to avoid misjudging edema as coagulation, yielding thresholds that differ in dependence from the time of determination.

In a clinical setting, dosimetry in each patient becomes crucial. To determine a therapeutically useful dose and the therapeutic window in individual patients based on slit lamp examination and additional angiography 1 hour after treatment bears the risk of overtreatment or unsuccessful treatment because the operating physician will seek to avoid collateral damage. Successful yet safe treatment could be achieved reproducibly if the treatment outcome could be monitored during the laser energy application. Considering the cell damage mechanism, selective RPE destruction was originally thought to be achieved by thermal necrosis of the cell.[5,14] However, recent investigations show that microbubble formation occurs around melanosomes in suspension with pulse durations within the nanosecond and microsecond regimen.[7–9] Calculations show that rapid vaporization is initiated when the melanosomes' surface temperature reaches approximately 150°C.[9] Brinkmann et al.[9] argued that cell death originates from microbubble formation, rather than thermal denaturation, after applying a train of microsecond pulses. We observed in a related

project that the thresholds for cell damage and bubble formation correlate well at pulse durations of up to 10 μs.[10] Bubble formation leads to a transient increase in backscattered light from the RPE that can be monitored using optical means to provide feedback as to whether RPE cells have been damaged [10–12]. Likewise, the onset of cavitation can be detected by acoustical means.[13] Thus, detecting bubble formation during the exposure can serve as immediate feedback, indicating that the angiographic endpoint (i.e., damage of RPE cells) has been reached. The result of the feedback can be used by the physician to adjust dosimetry manually. It is likewise conceivable that a device can be developed that automatically interrupts the treatment once RPE cell damage has been measured.

Outlook

Our ED_{50} threshold for scanning with 2.5-μs dwell time is 191 mJ/cm^2, similar to the threshold of 189 and 143 mJ/cm^2 that Framme et al.[17] measured in rabbits by using a spot diameter of approximately 100 μm with 5- and 1.7-μs pulses, respectively. Whether the scanning approach requires intrinsically higher radiant exposure compared with the pulse technique[23] is a subject for further investigation. Comparison of threshold values aside, the scanner bears several other advantages over pulsed systems. The laser scanner can be set up as a compact device that is entirely adapted to a targeting device, such as a slit lamp. In this study, we coupled a commercially available cw-laser via single mode fiber to the scanner. We are currently setting up a new scanning device that incorporates a compact cw-laser of 1.2-W output power into the slit lamp–adapted device, eliminating the need for optimizing the fiber coupling efficiency and increasing the available power at the cornea from 185 mW to approximately 700 mW. Future experiments, therefore, will be designed to investigate the extent of selectivity and the width of the therapeutic window for shorter exposure times. Most important, a scanner is able to create a variety of irradiation parameters, as opposed to the pulsed approach that can cover a small range of pulse durations with a fixed pattern. Furthermore, by scanning a small laser spot to produce spaced lines, a heat-diffusion geometry is introduced that allows selective RPE damage, even at exposure times that are significantly longer than the thermal relaxation time of the absorbing structures (Tables 1, 2). In contrast, the large spot diameter of the pulsed approach (approximately 100 μm in diameter) may lead to an unnecessary temperature increase in the center of the lesion and to heat diffusion into the photoreceptors; this possible outcome is indicated by the smaller therapeutic window of 1.9 that Framme et al.[17] determined in rabbits after 5-μs pulsed exposure. In fact, by changing the heat diffusion geometry introduced by different scan patterns, a scanner can control the extent of the selectivity. Selectivity is best achieved by irradiation with exposure times on the order of the thermal relaxation time and using separated lines (SEP). Thermal photocoagulation can also be realized using the same device, by slowing down the scan speed (i.e., increasing the dwell time) and using a scan pattern that facilitates heat conduction into the photoreceptors (INT). Thus, a scanner can serve both as a source for selective targeting and as a thermal photocoagulator.

Recovery of selective RPE lesion produced by the pulsed approach typically takes approximately 14 days.[5] By creating different RPE damage patterns and lesion sizes, the scanner will enable us to investigate whether the recovery time of the RPE defect can be accelerated. However, it remains to be shown whether the smaller area of recovering RPE after scanning SEP treatment is actually capable of removing existing edema or drusen. Future work will incorporate in vivo follow-up examinations regarding the restoration of the RPE barrier in the animal model.

Conclusions

In summary, selective targeting of the RPE is feasible with the use of a laser scanner with moderate laser power on the order of 100 mW. As indicated by the absence of ophthalmoscopically visible coagulation, irradiation with exposure times up to 15 μs seems to be safe, with a therapeutic window of at least 3.1 when using the SEP pattern. Selectivity has been confirmed by histology for up to 100 repetitive exposures of the SEP pattern at up to twice ED_{50} for 7.5- and 15-μs dwell times. With 30-μs irradiation, histology shows altered photoreceptors at $2\times$ ED_{50} and damaged photoreceptors at $3\times$ ED_{50}. Thus, 30-μs irradiation seems unsafe for selective targeting. Using the INT pattern, with which heat accumulation leads to a reduction of threshold radiant exposure, 15 μs was safe only with $<1.5\times$ ED_{50}. Therefore, for the INT pattern, irradiation with exposure times significantly longer than the thermal relaxation time should be avoided.

We have shown that the scanner can be useful in both selectively targeting the RPE and thermal photocoagulation. Adjustment of the dwell time and the applied scan pattern allows control if the heat diffusion geometry and extent of selectivity. Irradiating generously spaced locations with dwell times on the order of the thermal relaxation time is ideal for selective targeting; precision of individual RPE cell damage can be achieved. Slowing down the speed of the scanner (i.e., increasing the exposure time) and selecting a scan pattern that facilitates heat conduction into the photoreceptors is beneficial for thermal coagulation. Thus, thermal coagulation can be performed with the same device simply by adjusting the scanning parameters. Future experimental setups will incorporate a compact cw-laser on the targeting device as well as an online feedback system that monitors cell death during irradiation. Pending further experiments and eventual clinical trials, the scanning method may allow optimization of treatment parameters to individual patient's needs.

References

1. Birngruber R, Hillenkamp F, Gabel VP. Theoretical investigations of laser thermal retinal injury. *Health Phys*. 1985;48:781–796.
2. Lorenz B, Birngruber R, Vogel A. Quantifizierung der Wellenlängenabhängigkeit laserinduzierter Aderhauteffekte. *Fortschr Ophthalmol*. 1989;86:644–654.
3. Marshall J, Mellerio J. Pathological development of retinal laser photocoagulations. *Exp Eye Res*. 1968;7:225–230.
4. Wallow IH, Birngruber R, Gabel VP, Hillenkamp F, Lund OE. Netzhautreaktion nach Intensivlichtbestrahlung. *Adv Ophthalmol*. 1975;31:159–232.
5. Roider J, Michaud NA, Flotte TJ, Birngruber R. Response of the retinal pigment epithelium to selective photocoagulation. *Arch Ophthalmol*. 1992;110:1786–1792.
6. Gabel VP, Birngruber R, Hillenkamp F. Visible and near infrared light absorption in pigment epithelium and choroid. In: Shimizu K, ed. *International Congress Series No. 450, XXIII Concilium Ophthalmologicum, Kyoto*. Princeton, NJ: Excerpta Medica; 1978: 658–662.
7. Kelly WM, Lin CP. Microcavitation and cell injury in RPE cells following short-pulsed laser irradiation. *Proc SPIE*. 1997;2975: 174–179.
8. Lin CP, Kelly, MW. Cavitation and acoustic emission around laser-heated microparticles. *Appl Phys Lett*. 1998;72:2800–2803.
9. Brinkmann R, Hüttmann G, Rögener J, Roider J, Birngruber R, Lin CP. Origin of retinal pigment epithelium cell damage by pulsed laser irradiance in the nanosecond to microsecond time regimen. *Laser Surg Med*. 2000;27:451–464.
10. Lee H, Alt C, Pitsillides CM, Lin CP. Optical detection of intracellular cavitation during selective laser targeting of the retinal pigment epithelium: dependence of cell death mechanism on pulse duration. *J Biomed Optics*. In press.

11. Rögener J, Brinkmann R, Lin CP. Pump-probe detection of laser-induced microbubble formation in retinal pigment epithelium cells. *J Biomed Optics*. 2004;9:367–371.
12. Neumann J, Brinkmann R. Boiling nucleation on melanosomes and microbeads transiently heated by nanosecond and microsecond laser pulses. *J Biomed Optics*. 2005;10:024001
13. Schüle G, Ruhmor M, Hüttmann G, Brinkmann R. RPE damage thresholds and mechanisms for laser exposure in the microsecond-to-millisecond regimen. *Invest Ophthalmol Vis Sci*. 2005;46:714–719.
14. Roider J, Hillenkamp F, Flotte TJ, Birngruber R. Microphotocoagulation: selective effects of repetitive short laser pulses. *Proc Nat Acad Sci USA*. 1993;90:8643–8647.
15. Roider J, Brinkmann R, Wirbelauer C, Laqua H, Birngruber R. Retinal sparing by selective retinal pigment epithelial photocoagulation. *Arch Ophthalmol*. 1999;117:1028–1034.
16. Roider J, Brinkmann R, Wirbelauer C, Laqua H, Birngruber R. Subtreshold (retinal pigment epithelium) photocoagulation in macular diseases: a pilot study. *Br J Ophthalmol*. 2000;84:40–47.
17. Framme C, Schüle G, Roider J, Kracht D, Birngruber R, Brinkmann R. Threshold determinations for selective retinal pigment epithelium damage with repetitive pulsed microsecond laser systems in rabbits. *Ophthalmic Surg Lasers*. 2002;33:400–409.
18. Friberg TR, Karatza EC. The treatment of macular disease using a micropulsed and continuous wave 810-nm diode laser. *Ophthalmology.* 1997;104:2030–2038
19. Mainster MA. Decreasing retinal photocoagulation damage: principles and techniques. *Sem Ophthalmol*. 1999;14:200–209.
20. Moorman CM, Hamilton AM. Clinical applications of the Micro-Pulse diode laser. *Eye*. 1999;13:145–50.
21. Pollack JS, Kim JE, Pulido JS, Burke JM. Tissue effects of subclinical diode laser treatment of the retina. *Arch Ophthalmol.* 1998;116:1633–1639.
22. Berger JW. Thermal modeling of micropulsed diode laser retinal photocoagulation. *Lasers Surg Med.* 1997;20:409–415
23. Brinkmann R, Koop N, Özdemir M, et al. Targeting of the retinal pigment epithelium (RPE) by means of a rapidly scanned continuous wave (CW) laser beam. *Lasers Surg Med.* 2003;32:252–264.
24. Alt C, Framme C, Schnell S, Lee H, Brinkmann R, Lin CP. Selective targeting of the retinal pigment epithelium using an acousto-optic laser scanner. *J Biomed Optics.* 2005;10:064014
25. Framme C, Alt C, Schnell S, Brinkmann R, Lin CP. Selective Behandlung des RPE unter Verwendung eines gescannten CW-Laserstrahls im Kaninchenmodell. *Ophthalmologe*. 2005;102:491–496.
26. Birngruber R, Gabel VP, Hillenkamp F. Experimental studies of laser thermal retinal injury. *Health Phys*. 1983;44:519–531.
27. Finney DJ. *Probit Analysis.* 3rd ed. London: Cambridge University Press; 1971.
28. Sliney DH, Mellerio J, Schulmeister K. What is the meaning of thresholds in laser injury experiments?—implications for human exposure limits. *Health Phys*. 2002;82:335–347.
29. Wallow IH. Repair of the pigment epithelial barrier following photocoagulation. *Arch Ophthalmol*. 1984;102:126–135.
30. Del Priore LV, Glaser BM, Quigley HA, Green R. Response of pig retinal pigment epithelium to laser photocoagulation in organ culture. *Arch Ophthalmol*. 1989;107:119–122.